

Manuscript Number: AB-17-354R2

Title: Halloysite and chitosan oligosaccharide nanocomposite for wound healing

Article Type: Full length article

Keywords: halloysite, chitosan oligosaccharide, nanocomposite, wound healing, in vitro cell culture, in vivo murine model

Corresponding Author: Professor Giuseppina Sandri, PhD

Corresponding Author's Institution: University of Pavia

First Author: Giuseppina Sandri, PhD

Order of Authors: Giuseppina Sandri, PhD; Carola Aguzzi; Silvia Rossi; Maria Cristina Bonferoni; Giovanna Bruni; Cinzia Boselli; Antonia Icaro Cornaglia; Federica Riva; Cesar Viseras; Carla Caramella; Franca Ferrari

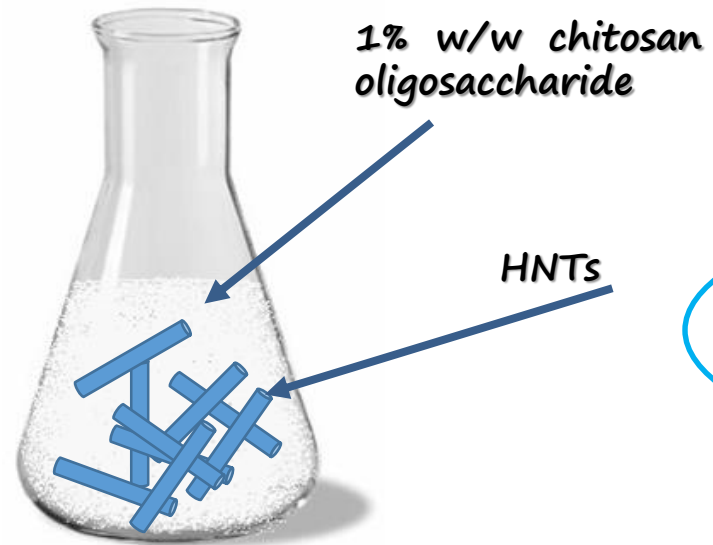
Abstract: Halloysite is a natural nanotubular clay mineral (HNTs, Halloysite Nano Tubes) chemically identical to kaolinite and, due to its good biocompatibility, is an attractive nanomaterial for a vast range of biological applications.

Chitosan oligosaccharides are homo- or heterooligomers of N-acetylglucosamine and D-glucosamine, that accelerate wound healing by enhancing the functions of inflammatory and repairing cells.

The aim of the work was the development of a nanocomposite based on HNTs and chitosan oligosaccharides, to be used as pour powder to enhance healing in the treatment of chronic wounds.

A 1:0.05 weight ratio HTNs/chitosan oligosaccharide nanocomposite was obtained by simply stirring the HTNs powder in a 1% aqueous chitosan oligosaccharide solution and was formed by spontaneous ionic interaction resulting in 98.6% w/w HTNs and 1.4% w/w chitosan oligosaccharide composition. Advanced electron microscopy techniques were considered to confirm the structure of the hybrid nanotubes.

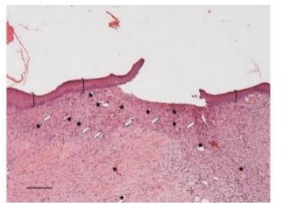
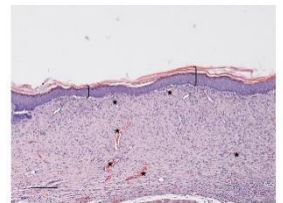
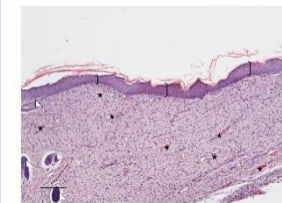
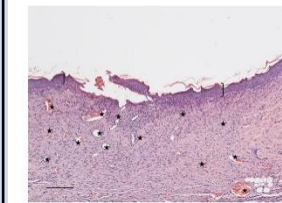
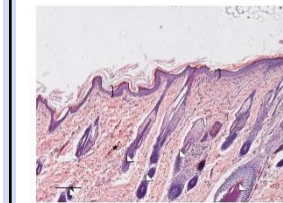
Both HTNs and HTNs/chitosan oligosaccharide nanocomposite showed good in vitro biocompatibility with normal human dermal fibroblasts up to 300 ug/ml concentration and enhanced in vitro fibroblast motility, promoting both proliferation and migration. The HTNs/chitosan oligosaccharide nanocomposite and the two components separately were tested for healing capacity in a murine (rat) model. HTNs/chitosan oligosaccharide allowed better skin reepithelization and reorganization than HNTs or chitosan oligosaccharide separately. The results suggest to develop the nanocomposite as a medical device for wound healing.



0.05 weight ratio  
chitosan oligosaccharide/HNTs  
nanocomposite (NC)

Chitosan oligosaccharide: 1.4% w/w  
HNTs: 98.6 % w/w

WOUND HEALING - HISTOLOGY - H&E  
(in vivo murine model)

	saline solution	HNTs	NC	Chitosan oligosaccharide	Intact skin
t=18					

Halloysite and chitosan oligosaccharide nanocomposite for wound healing

Giuseppina Sandri<sup>1\*</sup>, Carola Aguzzi<sup>2</sup>, Silvia Rossi<sup>1</sup>, Maria Cristina Bonferoni<sup>1</sup>, Giovanna Bruni<sup>3</sup>, Cinzia Boselli<sup>1</sup>, Antonia Icaro Cornaglia<sup>4</sup>, Federica Riva<sup>4</sup>, Cesar Viseras<sup>2,5</sup>, Carla Caramella<sup>1</sup>, Franca Ferrari<sup>1</sup>

<sup>1</sup>Department of Drug Sciences, University of Pavia, Viale Taramelli 12, 27100 Pavia, Italy

<sup>2</sup>Department of Pharmacy and Pharmaceutical Technology, University of Granada, Campus of Cartuja, Granada, 18071 s/n, Spain

<sup>3</sup>Department of Chemistry, Physical Chemistry Section, University of Pavia, Viale Taramelli 16, 27100 Pavia, Italy

<sup>4</sup>Department of Public Health, Experimental and Forensic Medicine, University of Pavia, via Forlanini 2, 27100 Pavia, Italy

<sup>5</sup>Andalusian Institute of Earth Sciences, CSIC-University of Granada, Armilla, Granada, Spain

\*Corresponding author:

Prof. Giuseppina Sandri,

Department of Drug Sciences,

University of Pavia,

Viale Taramelli 12, 27100 Pavia, Italy

Tel: 0039 0382 987728

Fax: 0039 0382 422975

E-mail address: giuseppina.sandri@unipv.it

## Abstract

Halloysite is a natural nanotubular clay mineral (HNTs, Halloysite Nano Tubes) chemically identical to kaolinite and, due to its good biocompatibility, is an attractive nanomaterial for a vast range of biological applications.

Chitosan oligosaccharides are homo- or heterooligomers of N-acetylglucosamine and D-glucosamine, that accelerate wound healing by enhancing the functions of inflammatory and repairing cells.

The aim of the work was the development of a nanocomposite based on HNTs and chitosan oligosaccharides, to be used as pour powder to enhance healing in the treatment of chronic wounds.

A 1:0.05 weight ratio HTNs/chitosan oligosaccharide nanocomposite was obtained by simply stirring the HTNs powder in a 1% aqueous chitosan oligosaccharide solution and was formed by spontaneous ionic interaction resulting in 98.6% w/w HTNs and 1.4% w/w chitosan oligosaccharide composition. Advanced electron microscopy techniques were considered to confirm the structure of the hybrid nanotubes.

Both HTNs and HTNs/chitosan oligosaccharide nanocomposite showed good *in vitro* biocompatibility with normal human dermal fibroblasts up to 300 µg/ml concentration and enhanced *in vitro* fibroblast motility, promoting both proliferation and migration. The HTNs/chitosan oligosaccharide nanocomposite and the two components separately were tested for healing capacity in a murine (rat) model. HTNs/chitosan oligosaccharide allowed better skin reepithelization and reorganization than HNTs or chitosan oligosaccharide separately. The results suggest to develop the nanocomposite as a medical device for wound healing.

Keywords: halloysite, chitosan oligosaccharide, nanocomposite, wound healing, in vitro cell culture, in vivo murine model

## 1. Introduction

Cutaneous wounds represent a major issue in medical care, with approximately 300 million chronic and 100 million traumatic wound patients worldwide, The incidence of chronic wounds is likely to dramatically increase as long as the population ages due to the rising prevalence of type 2 diabetes, peripheral vascular disease and metabolic syndrome. This will have a huge impact on financial burden of health-care systems worldwide [1]. Whereas the treatment strategies adopted for acute and limited area traumatic wounds are effective, the problems arise in the long-term care of patients with large area burns, infected and severe chronic wounds.

Skin serves as protective barriers against the outside world, therefore any break in this barrier must be mended rapidly. Wound healing process is based on various phases, typically haemostasis, inflammation, proliferation and remodelling, and depends on many factors, involving multiple cell populations and extracellular matrix (ECM) bioactive molecules as soluble mediators [2]. During inflammation, inflammatory cells (neutrophils, activated monocytes and macrophages), are recruited at the site of injury and release proinflammatory cytokines, such as tumor necrosis factor  $\alpha$  (TNF  $\alpha$ ), interleukines IL-1 and IL-6, and growth factors, such as transforming growth factor  $\beta$  (TGF  $\beta$ ) and insulin like growth factor (IGF) [3, 4]. These bioactive molecules coordinate the transition from inflammatory to proliferating phase. The length and the severity of the inflammation phase ultimately dictates the quality of repaired tissue. During the proliferative phase, the granulation tissue is deposited and fibroblasts and endothelial cells migrated into the wound. Since fibroblasts produce collagen based extracellular matrix (ECM) reepithelialisation of the wound occurs and keratinocytes migrate into the wound from wound margins covering the neoformed tissue. After that the remodelling occurs and disorganized collagen III is substituted by collagen I bundles. The objective of wound managements is to heal the wound in the shortest time to prevent infection and to minimize pain, discomfort and scarring. Traditional wound management relied on simple materials such as gauze according to the principle “to cover and conceal” [5]. A more recent approach is to promote healing by using smart dressings able to enhance the formation of viable tissue *in vivo* [5].

Recently clay minerals have been proposed as substrates and matrices to enhance stem and progenitor cell proliferation and differentiation, thus representing an innovative platform for tissue regeneration and biomaterial design [6, 7]. Moreover, cells could interact with clays suggesting new opportunities for functionalization of surfaces for enhanced reparative response. The combination of polymers/oligomers with clay minerals to obtain nanocomposites provides a further opportunity to develop new functional materials. Recently, biomedical applications of nanoclay-polymer composites have been rapidly increasing as antimicrobial coatings and bone healing implants [8].

Halloysite is a tubular aluminosilicate with hollow structure: it is formed by 10-15 aluminosilicate layers of 0.7 nm thick kaolin sheet rolled to form a hollow cylinder. It has a negatively charged outer surface and a positively charged inner lumen with an outer overall diameter of 40-70 nm with a length of 0.4 to 1.5  $\mu\text{m}$ . Halloysite can adopt different forms including elongated tubes, short tubes, spheroidal squat cylinders and plates: the nanotubular and the spheroidal forms are the most common ones [9]. Halloysite nanotubes (HNTs) are a safe and biocompatible material [8], apparently able to stimulate processes related to cell growth and proliferation [10, 11]: the shorter dimension of HNTs (2  $\mu\text{m}$  in length) in comparison to asbestos

fibers (several tens of microns) allows their removal by macrophages [12]. HNTs based nanocomposites have been mainly described in literature as materials with improved mechanical and thermal properties [12] and carriers of drugs including biomacromolecules such as proteins and DNA [12, 13]. Moreover tube end capped systems have been developed to optimize the release rate of bioactive molecules [12, 14]. In particular Dзамukova et al. have proposed an enzyme activated system for the intracellular drug delivery [15]. HNTs nanomposites have been studied by using different microscopy techniques: SEM, TEM and AFM which also allow to visualize the rolling alumosilicate sheets [14, 16-18].

Chitosan oligosaccharides are hetero- or homo-oligomers of D- acetylglucosamine and D-glucosamine. They are able to accelerate wound healing by enhancing the functions of inflammatory and repairing cells having anti-inflammatory and immunostimulating activities [19]. Moreover chitosan oligosaccharides possess antioxidant activity involving free radical scavenging and the induction of antioxidative enzyme expression [20].

Given these premises, the aim of the work was the development of a nanocomposite based on HTNs nanotubes and chitosan oligosaccharide, to be used as pour powder to enhance healing and to prevent infections in the treatment of chronic wounds. The HTNs/chitosan oligosaccharide nanocomposite was tested for in vitro biocompatibility towards fibroblasts and in vitro wound healing properties to evidence fibroblast proliferation and migration. Moreover the HTNs/chitosan oligosaccharide wound healing efficacy was tested in aa murine (rat) model.

## 2. Experimental part

### 2.1. Materials

The nanocomposites has been prepared by using:

- clay mineral: halloysite nano tubes (HTNs) premium grade (New Zealand China Clays Ltd. Auckland, NZ);
- chitosan oligosaccharide (average molar mass=1000 Da, with 75.4% deacetylation degree (Heppe Medical Chitosan GmbH, Halle, Germany).

### 2.2. Methods

#### 2.2.1. HTNs/chitosan oligosaccharide nanocomposites preparation (NC)

HTNs/chitosan oligosaccharide nanocomposites were prepared by simple solid liquid interactions [21-23].

Known amounts of clay mineral powder (0.1 to 2 g) were dispersed in 10 ml chitosan oligosaccharide aqueous solution (1% w/w). The resulting dispersions were shaken at 150 rpm for 24 hours in a water bath

(Falc Instruments, I) at room temperature and the solid phases were subsequently recovered by centrifugation at 22000 rpm for 30 min (Jouan K22i, Italia), frozen at -20°C for 24 h and freeze-dried for 24 h (Heto 15, Analitica De Mori, I). Table 1 reports the HTNs/chitosan oligosaccharide ratio (R), and the theoretical composition of the prepared nanocomposites obtained with HTNs/chitosan oligosaccharide. Actual composition is also given (see 2.2.2.1)

## 2.2.2. Nanocomposite characterization

### 2.2.2.1. Composition

Chitosan oligosaccharide was quantified by means of a ninhydrin assay modified from Leane et al. [24] and Sandri et al. [23]. A calibration curve was prepared by using chitosan oligosaccharide aqueous solutions at the following concentrations: 0.75, 0.5, 0.25 and 0.1 w/w. Each sample was diluted 1:1 v/v with 2 ml of the ninhydrin reagent (ninhydrin 2% w/v, hydrindantin 6.8 mg/l in 3:1 v/v DMSO:lithium acetate buffer 4 M, pH 5.2; Sigma-Aldrich, I) under nitrogen blanket. Each sample was placed in a shaking bath at 100°C for 8 min. The vials were then vortexed for 15 s in order to oxidize the hydrindantin excess. After cooling, each sample was diluted 1:10 v/v with a 1:1 ethanol:water mixture and the absorbance was assayed at 570 nm (Lamba 25 spectrophotometer, Perkin Elmer, I). The calibration curve was linear ( $R^2 \geq 0.9995$ ) in the chitosan glutamate concentration range 0.75 – 0.1% w/w.

### 2.2.2.2 Physical-chemical characterization

#### 2.2.2.2.1. FT-IR

FT-IR spectra were obtained using a Nicolet FT-IR iS10 Spectrometer (Nicolet, Madison, WI, USA) equipped with ATR (Attenuated Total Reflectance) sampling accessory (Smart iTR with ZnSe plate) by co-adding 256 scans in the 4000–650 cm<sup>-1</sup> range at 4 cm<sup>-1</sup> resolution.

#### 2.2.2.3.2. Thermal analysis

Thermal characterization was carried out using a DSC Q2000 apparatus interfaced with a TA 5000 data station (TA Instruments, NewCastle, DE, USA). The DSC instrument was calibrated using ultrapure (99.999%) indium (melting point = 156.6 °C;  $\Delta H = 28.54 \text{ J g}^{-1}$ ) as standard. The calorimetric measurements were carried out in open standard aluminium pans under nitrogen flow (45 mL·min<sup>-1</sup>) at 10 K·min<sup>-1</sup>.

#### 2.2.2.3.3. X-ray powder diffraction (XRPD)

XRPD measurements were performed using a D5005 Bruker diffractometer (Karlsruhe, Germany) (CuK $\alpha$  radiation,  $\lambda(K\alpha_1) = 1.54056 \text{ \AA}$ ; voltage of 40 kV and current of 40 mA) equipped with a  $\theta$ - $\theta$  vertical goniometer, Ni filter, monochromator and scintillator counter. The patterns were recorded at room temperature in step scan mode (step size:  $0.020^\circ$ , counting time: 3 s per step) in the  $5 < 2\theta < 35$  angular range.

### 2.2.2.3. Microscopy

#### 2.2.2.3.1. Energy filtered transmission electron microscopy (EFTEM) and electron energy loss spectroscopy (EELS)

The samples were deposited on a carbon coated Cu grid and examined using a LIBRA 120 PLUS EFTEM instrument equipped with in-column corrected OMEGA Filter, operating at an acceleration voltage of 120 kV. Optimum amplitude contrast was achieved using lens aperture of 30  $\mu\text{m}$ , and afterward removing inelastic electrons by zero-loss filtering in the elastic scattering image (ESI) mode. Simultaneous EELS was performed on selected areas of the samples.

#### 2.2.2.3.2. Ultra-high resolution transmission electron microscopy (UHRTEM) and analytical electron microscopy (AEM)

Chitosan oligosaccharide /HNTs nanocomposites were analyzed by UHRTEM using a FEI Titan G2 60-300 microscope with a high brightness electron gun (X-FEG) operated at 300 kV and equipped with a Cs image corrector (CEOS) and for AEM a SUPER-X silicon-drift windowless energy-dispersive X-ray spectroscopy (EDX) detector. The AEM spectra were collected in STEM (Scanning Transmission Electron Microscopy) mode using a HAADF (High Angle Annular Dark Field) detector. X-ray chemical element maps were also collected.

Electron microscopy images were analyzed using Image Pro Plus® software and Gaussian fitting to obtain quantitative information about the morphological features. Both internal and external diameters of the pristine and coated nanotubes were measured. At least 100 particles were counted from multi-picture in each case. Aspect ratio was calculated as the ratio between width (length) and height (diameter).

#### 2.2.2.4 Particle size and Zeta potential



Particle size (PS) and polydispersity index (PI) were measured at 25°C by Photon Correlation Spectroscopy (N5, Beckman Coulter) at an angle of 90° after sample dispersion/dilution in bidistilled and filtered (0.45 µm) water.

Z-potential of NC suspension was carried out at 25°C by means of a Malvern Zetasizer Nano ZS90 (Malvern Ltd., UK). HNTs suspension and chitosan oligosaccharide solution having the same concentration as in NC were also tested.

### 2.2.3. In vitro biocompatibility

#### 2.2.3.1 Cytotoxicity test

Normal Human Dermal Fibroblasts (NHDF) from juvenile foreskin (PromoCell GmbH, G) were used. Cells between the 2<sup>nd</sup> and 5<sup>th</sup> passage were employed for all the experiments. Fibroblasts were grown in Dulbecco's modified Eagle medium (DMEM, Lonza, I), supplemented with 10% fetal calf serum (FCS, Euroclone, I) and 200 IU/ml penicillin-0.2 mg/ml streptomycin (PBIinternational, I), kept at 37°C in a 5% CO<sub>2</sub> atmosphere with 95% relative humidity (RH).

Fibroblasts were seeded in each well of 96-well plates (area 0.34 cm<sup>2</sup>) at a density of 10<sup>5</sup> cells/cm<sup>2</sup>. Cells were grown 24 h to obtain sub-confluence.

Then cells were washed with saline solution and the cell substrates were put in contact with the samples.

In a first set of experiments HNTs biocompatibility was assessed after 3 and 24 h contact.

Subsequently cell substrates were put in contact with 0.05 HNTs/chitosan oligosaccharide nanocomposite suspended in growth medium at 300 µg/ml concentration for HNTs and 4 µg/ml for chitosan oligosaccharide.

HNTs at 300 µg/ml concentration and chitosan oligosaccharide at 4 µg/ml were evaluated for comparison.

The samples were put in contact with the fibroblasts either for 3 or 24 h. Growth medium (GM) was used as control. Subsequently, the MTT test was performed. This test is based on the activity of mitochondrial dehydrogenases of vital cells that convert MTT to formazan. 125 µl of MTT solution (Sigma Aldrich, I) at 0.25 µg/ml concentration in HBSS (Hank's Buffered Salt Solution) pH 7.4 was put in contact with each sample for 3 h. The reagent was then removed from each well and the cells were washed with PBS (150 µl) to remove the samples and un-reacted MTT solution. After PBS removal, 100 µl of DMSO were put in each well and the absorbance was assayed at 570 nm by means of an ELISA plate reader (Imark Absorbance Reader, Biorad, I), with a reference wavelength set at 655 nm. Cell viability was calculated as % ratio between the absorbance of each sample and the absorbance of the cells kept in contact with the control.

### 2.2.3.2. Proliferation test

$2 \cdot 10^4$  fibroblasts/well were simultaneously co-seeded with the samples in each well of a 96- well plate. The following samples were tested: a 0.05 HTNs/chitosan oligosaccharide nanocomposite suspension in growth medium (corresponding to 300  $\mu\text{g/ml}$  concentration in HTNs and 4  $\mu\text{g/ml}$  in chitosan oligosaccharide), a HTNs suspension at 300  $\mu\text{g/ml}$  concentration and a chitosan oligosaccharide suspension at 4  $\mu\text{g/ml}$ , both tested for comparison. Growth medium (GM) was used as control.

The well plate was kept at 37°C in a 95% air/ 5% CO<sub>2</sub> atmosphere at 95% relative humidity for 24 h. After 24 h, the cells were subconfluent and attached to the well bottom and MTT test was performed as previously described.

### 2.2.3.3. Cell migration/proliferation assay for wound healing

The gap closure cell migration/proliferation assay was performed according to a previously described procedure [23]. The assay employs Petri  $\mu$ -Dishes (35 mm, Ibidi, Giardini, I) which contain a special insert consisting of two cell grow chambers (growth area: 0.22 cm<sup>2</sup> each) divided by a septum (500  $\mu\text{m} \pm 50 \mu\text{m}$ . in width) simulating a cell free gap.

Fibroblasts were seeded in each chamber at 10<sup>5</sup> cells/cm<sup>2</sup> concentration and grown at confluence in standard conditions as described in 2.3.3 section. After 24 h, cells reached confluence and the insert was removed displaying two areas of cell substrates divided by the gap. The cell substrates were put in contact with 200  $\mu\text{l}$  of either 0.05 nanocomposite, or HNTs or chitosan oligosaccharide at the concentrations given in 2.2.2.3. Cells kept in contact with growth medium were used as control. At prefixed time intervals (0, 24, 48 and 72 h), microphotographs were taken to evaluate the cell migration in the gap.

To differentiate between simple migration and proliferation, cell proliferation properties were verified by assessing 5-Bromo-2'-Deoxyuridine (BrdU) incorporation in DNA synthesis . At this purpose during the last hour of culture, cells were labeled by adding 30 mM BrdU (Sigma-Aldrich) to the medium; then the samples were washed with PBS and fixed in 70% ethanol. Incorporated BrdU was detected by immunostaining reaction with anti-BrdU antibody (Amersham Bioscience, Milan, Italy) as follows: the substrates were washed with PBS and incubated with HCl 2N for 30 min at room temperature. Samples were neutralized in 0.1 M sodium tetraborate (pH 8.5) for 15 min, washed twice for 5 min in PBS, and incubated for 20 min in a PTA blocking solution (1% w/v BSA and 0.02% w/v Tween20 in PBS). Cells were then incubated for 1 h with mouse anti-BrdU antibody, diluted 1:100 w/v in PTA solution, washed 3 times (10 min each) with the same

solution, and then incubated for 30 min in PTA solution containing anti-mouse IgG FITC-antibody (Sigma-Aldrich, 1:100 w/v dilution). Finally, cell substrates were again extensively washed with PBS, counterstained for DNA with 0.5 mg/ml Hoechst 33258 (Sigma-Aldrich), and mounted in Mowiol (Sigma-Aldrich). Cells were scored for BrdU immunofluorescence positivity with a Zeiss Axiophot fluorescence microscope (Carl Zeiss, Oberkochen, Germany). Each experiment was repeated 3 times. All the cells grown into the gaps were counted. All the green labelled cells (BrdU positive) represented the proliferated cells and the difference between the blue labelled cells (Hoechst 33258 positive) and the green labelled cells represented the migrated cells.

#### 2.2.4. In vivo wound healing efficacy in the rat model

All animal experiments were carried out in full compliance with the standard international ethical guidelines (European Communities Council Directive 86/609/EEC) approved by Italian Health Ministry (D.L. 116/92). The study protocol was approved by the Local Institutional Ethics Committee of the University of Pavia for the use of animals. 6 male rats (Wistar 200–250 g) were anesthetized with equitensine at 3 ml/kg (39 mM pentobarbital, 256 mM chloral hydrate, 86 mM MgSO<sub>4</sub>, 10% ethanol v/v, and 39.6% propyleneglycol v/v) and shaved to remove all hair from their backs. Three circular full thickness burns, having a diameter of 4 mm, were produced on the back of the animals by contact with an aluminum rod (105°C for 40 s). 24 hours later, the formed blisters were removed using a 4-mm diameter biopsy punch to obtain a full-thickness lesions. Either 30 mg of HNTs, or 0.4 mg of chitosan oligosaccharide or 30.4 mg of NC were applied to the lesions and each powder was wetted with 20 µl of saline solution (0.9 g/l). Lesions treated with 20 µl of saline solution were the negative control. Lesions were covered with a sterile gauze and the rats' back was wrapped with a surgery stretch (Safety, Monza, Italy) to protect lesions. At prefixed times after blister removal (0, 3, 7, 10, 14 and 18 days) photographs of the lesions were taken by using a digital camera (Sigma SD 14) which allowed for sizing the lesions and monitoring the healing process. The treatments were repeated after each shot. The dimensions of wounded area were acquired with an image analysis software (ICY, Institute Pasteur, Paris, France). 18 days after the treatment full thickness biopsies were taken in correspondence of the initial lesions and the histological analysis of the excised tissues was performed. A biopsy of intact skin was also taken for comparison.

#### 2.2.5. Histological analysis

A histological examination of the full thickness biopsies was performed after 18 days treatment. The animals were sacrificed and tissue samples were bisected along the widest line of the wound, and then fixed in 4% w/v neutral buffered paraformaldehyde for 48 h, dehydrated with gradient alcohol series, cleared in xylene and embedded in paraffin. Sections (8  $\mu\text{m}$ ) were obtained using a Leitz microtome (Wetzlar, Germany) and were stained with haematoxylin and eosin (H&E). The slices were examined at the magnification of 5x under a light microscope Axiophot Zeiss (Oberkochen, Germany) equipped with a digital camera.

#### 2.2.6. Statistical analysis

Statistical differences were evaluated by means of a non-parametric test: Mann Whitney (Wilcoxon) W test, (Stat Graphics 5.0, Statistical Graphics Corporation, MD, USA). Differences were considered significant at  $p < 0.05$ ; only significant differences are reported in the captions of the relevant table/figures.

### Results and discussion

#### 3.1 System characterization

In Table 1 the composition (chitosan oligosaccharide and HTNs %) of the nanocomposites prepared is given. Figure 1 shows the percentage of chitosan oligosaccharide associated to HNTs as a function of chitosan oligosaccharide/HTNs weight ratio. An increase in chitosan oligosaccharide/HTNs weight ratio caused a significant decrease in the % of chitosan oligosaccharide association to form the nanocomposite up to 0.075 weight ratio. Figure 2 shows the percentage of chitosan oligosaccharide in chitosan oligosaccharide/HTNs nanocomposite as a function of chitosan oligosaccharide/HTNs weight ratio. The chitosan oligosaccharide percentage significantly increased on increasing the chitosan oligosaccharide/HTNs weight ratio up to a maximum in correspondence to 0.05 chitosan oligosaccharide/HTNs weight ratio, thereafter an increase in chitosan oligosaccharide/HTNs weight ratio caused a significant decrease in chitosan oligosaccharide percentage in the nanocomposite.

The FT-IR, DSC and XRPD techniques were used to study the solid state properties of the components and the composite and to elucidate the interaction between chitosan oligosaccharide and HNTs (data not shown). However, the percentage of chitosan oligosaccharide in NC was too low (1.4% w/w) to be detected with these techniques. In particular NC FT-IR spectrum was dominated by the HNTs absorption peaks, whereas the peaks and bands typical of chitosan oligosaccharide were not visible. Similarly, the glass transition present in the chitosan oligosaccharide thermogram disappeared in that of NC. Furthermore, since chitosan oligosaccharide is amorphous, its presence in NC diffractogram could not be detected.

Advanced electron microscopy techniques were considered to confirm the structure of pristine halloysite and the nanocomposites. The halloysite particles were predominantly cylindrical and open-ended, with an electron-transparent central lumen, clearly observed in circular tube cross-sections with a calculated aspect ratio of 10. As already reported by Cravero et al. [9], the presence of spheroidal, prismatic and onion-like particles was also observed even if in minor proportion.

The microphotograph in Figure 3 reveals three areas with different transparency to the electrons. From outside to inside it is possible to distinguish a zone of low opacity that may be due to a chitosan oligosaccharide layer coating the HNTs nanotube surface, followed by a darker area, corresponding to the rolled aluminosilicate sheets and finally the inner lumen of the tube (more transparent). The thickness of the polymer layer is ~50 nm. The measured internal and external diameters were  $28 \pm 5.1$  nm and  $70 \pm 8.3$  nm for pristine HNTs and  $26 \pm 2.2$  nm and  $125 \pm 12.7$  nm for coated HNTs.

The C K EELS spectrum obtained in the area formed by the circle indicated in the microphotography is also included in Figure 3. The EELS spectrum is typical of amorphous carbon, with an initial C K peak at 285 eV and a second and more intense peak at ~ 290 eV (Garvey et al., 1994). Unfortunately, the equipment did not allow punctual analysis hindering differentiation between amorphous carbon of the grid and that of the chitosan coating.

To confirm the hybrid nature of the chitosan oligosaccharide/ HNTs, UHRTEM images coupled with XEDS analysis and digital X-Ray maps were used (Figure 4). Figure 4A shows typical hybrid nanotubes with external diameters up to 250 nm and length of 500-1500 nm. The observed diameters are clearly higher than those of pristine halloysite nanotubes (~ 100 nm), as a result of the chitosan coating. Figure 4B shows a HAADF image in which XEDS analysis was performed on five selected areas. XEDS spectra of the different studied areas showed in all cases peaks deriving both from HNTs (O, Al and Si) and chitosan oligosaccharide (N, C and O) (only spectrum of area 1 is shown). In Figures 4C to 4F, X-ray maps of elements are shown, making evident the homogeneous distribution of organic and inorganic matters on the nanotubes.

HNTs was characterized by an unimodal size having mean particle diameter of  $470.7 \pm 7.5$  nm and a polydispersion index of  $0.296 \pm 0.021$ , whereas chitosan oligosaccharide/HNTs nanocomposite showed an unimodal distribution with particle size of  $497.1 \pm 3.7$  nm, significantly higher than that of HNTs, and polydispersion index of  $0.211 \pm 0.051$ .

HNTs suspension was characterized by negative zeta potential of  $-17.6 \pm 1.7$  mV in accordance with literature [25], chitosan oligosaccharide was characterized by positive zeta potential of  $7.3 \pm 0.2$  mV while the

nanocomposite has negative zeta potential of  $-4.18 \pm 0.3$  mV higher than that of HNTs pristine to confirm the chitosan oligosaccharide deposition onto the outer region of halloysite nanotubes.

Chitosan oligosaccharide is a polycation freely soluble in aqueous medium while HNTs presents a negatively charged surface due to isomorphous substitution of  $Al^{3+}$  for  $Si^{4+}$ . Therefore chitosan oligosaccharide likely interacts with HNTs to form the nanocomposite by electrostatic interaction between chitosan oligosaccharide cationic amine groups and HNTs negatively charged outer surface. Moreover, the amine and hydroxyl groups of chitosan oligosaccharide can interact with the Si-O groups of HNTs via hydrogen bonding. The nanocomposite characterization supports that HNTs are coated by chitosan oligosaccharide. This behavior has already been reported in the literature for chitosan [26].

### 3.2. In vitro biocompatibility

Figure 5 reports the in vitro cytotoxicity results (expressed as % cell viability) of HNTs (concentrations ranging from 10 to 300  $\mu\text{g/ml}$ ) after 3 or 24 h contact time with fibroblasts.

After 3 h contact, the % viability of fibroblasts was significantly lower than the control (Growth medium GM) and only the 150  $\mu\text{g/ml}$  concentration allowed for cell growth as much as GM. On the contrary, after 24 h contact, HNTs, at all concentrations, allowed cell growth as much as GM, which indicates that HNTs did not cause any significant modifications in cell behavior. The difference in results between the two contact times could be due to the physical/spatial interference of HNTs nanotubes due to their a high aspect ratio: after 24 h contact, cell adaptability to the solid particles might have occurred thus allowing for a cell growth similar to the one occurring in normal growth condition (GM). 24 h was considered a standard time suitable to predict in vitro cytotoxicity considering the fibroblast cell cycle (24 h). The 300  $\mu\text{g/ml}$  HNTs maximum concentration maximum tested was selected to continue the characterization.

Figure 6 shows the in vitro cytotoxicity results after 3 or 24 h contact time and in vitro proliferation (% viability) results for 0.05 chitosan oligosaccharide / HNTs nanocomposite NC (HNTs concentration 300  $\mu\text{g/ml}$  and chitosan oligosaccharide concentration 4  $\mu\text{g/ml}$ ), HNTs (maximum concentration 300  $\mu\text{g/ml}$ ) and chitosan oligosaccharide (concentration 4  $\mu\text{g/ml}$ ), towards fibroblasts.

After 3 h, NC and chitosan oligosaccharide allowed for a % cell viability significantly higher than that observed for HNTs and even higher than that observed for GM. After 24, HNTs had the same performance, not significantly different, in cell growth as GM. The % viability was significantly higher for NC and chitosan oligosaccharide than that observed for GM: during this time frame cells were able to undergo mitosis and

consequently, the presence of chitosan oligosaccharide and NC enhanced cell growth to a higher extent with respect to GM. These results were supported by the proliferation test. In particular, since in this test the cells and the samples were co-seeded, it was possible to investigate the capability of the sample to modify not only cell growth but also cell attachment, which represents a crucial event in cell cycle. In particular, NC showed a proliferation (% viability) close to 100% and not significantly different from GM.

Figure 7 shows the microphotographs of cell substrates subjected to in vitro wound healing test and put in contact with 0.05 chitosan oligosaccharide/ HNTs nanocomposite (HNTs concentration 300  $\mu\text{g/ml}$  and chitosan oligosaccharide concentration 4  $\mu\text{g/ml}$ ), HNTs (concentration 300  $\mu\text{g/ml}$ ), chitosan oligosaccharide (concentration 4  $\mu\text{g/ml}$ ) and GM growth medium (standard growth conditions). At starting point, all cell substrates clearly showed empty gaps surrounded by two confluent growth areas. After 24 h, the gaps started to be populated by fibroblasts and after 48 h in all cases, fibroblasts completely filled the gaps even if the growth was not at confluency. The presence of particles, clearly visible under optical microscopy, made of either HNTs or chitosan oligosaccharide / HNTs nanocomposite did not impair or slow down the cell growth, confirming the viability results.

Since fibroblasts are migrating cells, Br deoxyuridine test was associated to in vitro wound healing test to identify and count the cells which were in proliferating phase (S-phase) (positively green and blue stained) while filling the gaps.

Figure 8 shows the percentages of migrated (blue stained cells) and proliferating cells (blue and green stained cells) counted in the gaps at the end of in vitro wound healing test, after 72 h growth.

All samples (0.05 chitosan oligosaccharide / HNTs nanocomposite (NC having 300  $\mu\text{g/ml}$  concentration of HNTs and 4  $\mu\text{g/ml}$  concentration of chitosan oligosaccharide), HNTs (concentration 300  $\mu\text{g/ml}$ ), chitosan oligosaccharide (concentration 4  $\mu\text{g/ml}$ ) and the growth medium GM (standard growth conditions) displayed a remarkable presence of fibroblasts in the gaps with high percentages of migrated cells and low percentages of proliferating cells. In particular, HNTs showed a significantly lower capability to enhance cell proliferation, chitosan oligosaccharide had the same performance as GM, while NC performed at the best, allowing for a significantly higher percentage of migrated cells.

Figure 9 shows the microphotographs of cell substrates that were subjected at the same time to in vitro wound healing test and Br-deoxyuridine test (blue stained cells =migrated cells; blue and green stained cells =proliferating cells in S-phase). The photographs of the gaps were taken after 72 h of growth at the end of in vitro wound healing test. The gap images visually confirm the results of the quantitative test showing the

presence of a higher number of green stained fibroblasts in NC sample with respect to those observed in the other samples.

### 3.3. In vivo wound healing efficacy on rat model

Figure 10 shows the in vivo lesion size reduction vs time profile evaluated for 0.05 chitosan oligosaccharide / HNTs nanocomposite (NC having 300  $\mu\text{g/ml}$  concentration of HNTs and 4  $\mu\text{g/ml}$  concentration of chitosan oligosaccharide), HNTs (concentration 300  $\mu\text{g/ml}$ ), chitosan oligosaccharide (concentration 4  $\mu\text{g/ml}$ ) and saline solution, as negative control.

All the samples caused a significant reduction in the lesion area width. Although there were no significant differences in performance between the different samples, NC allowed for the lowest lesion area vs time profile and interestingly the profile was almost flat up to 10 days without any enlargement of the lesion conceivably due to the inflammatory response. HNTs, chitosan oligosaccharide and saline solution showed almost superimposable profiles with a slight increase in lesion area between 7 and 10 days of treatment.

Figure 11 shows the light microphotographs of haematoxylin and eosin stained skin sections after 7 and 18 days of treatment with saline solution (negative control), HNTs, NC and chitosan oligosaccharide. Intact skin section is also reported for comparison.

After 7 day treatment, the lesion that had being contact with NC, showed an early phase re-epithelialization, which was limited to the lesion borders. Hemostasis had occurred by formation of platelet plug, neutrophil and macrophage infiltrate had removed dead fibrin tissue while neoangiogenesis had reconstructed the vasculature in damaged areas. Moreover, the presence of granulation tissue (macrophages, lymphocytes and fibroblasts) which, through the production of chemotactic factors for fibroblasts and the promotion of mesenchymal cell proliferation, plays a crucial role in wound healing, was detected.

HNTs and chitosan oligosaccharide had achieved hemostasis by formation of platelet plug, but large, disrupted blood vessels were still present just beneath the surface. Neoangiogenesis as well as granulation tissue were detected only in some areas. The negative control (saline solution) had allowed platelet plug formation but left behind large areas with disrupted blood vessels.

Although all samples proved to be more effective than saline solution, NC treatment for 7 days was performing better than chitosan oligosaccharide and HNTs treatments in promoting advanced angiogenesis. After 18 days of treatments all samples and also saline solution allowed for complete re-epithelialization with the presence of reorganized collagen bundles, but in the case of saline solution, the neoformed epithelium had insufficient robustness as evidenced by a clear fracture in the epithelium. NC treatment confirmed



capable of healing the lesion more rapidly than other treatments, also because the dermal layer showed the regeneration of hair follicles with an overall structure practically identical to that of intact skin.

#### 4. Conclusions

A nanocomposite made of chitosan oligosaccharide/halloysite with a chitosan oligosaccharide / HNTs weight ratio of 0.05 was successfully prepared and characterized; such a ratio allowed the maximum association of chitosan oligosaccharide to HNTs to be obtained in the nanocomposite. Advanced electron microscopy techniques allowed the structure of the hybrid nanotubes to be confirmed: the chitosan oligosaccharide - HNTs association was likely induced by of the electrostatic interaction between chitosan oligosaccharide cationic amine groups and HNTs negatively charged outer surface and the formation of hydrogen bonding between chitosan oligosaccharide amine and hydroxyl groups and HNTs Si-O groups.

Chitosan oligosaccharide / HNTs nanocomposite proved to be biocompatible *in vitro* towards normal human dermal fibroblasts and, in an *in vitro* wound healing test, enhanced *in vitro* cell proliferation (cells in S-phase) rather than simple fibroblast migration.

The *in vivo* wound healing murine model definitely supported the performance of chitosan oligosaccharide / HNTs nanocomposite in promoting wound healing. Indeed, after 7 days of treatment, although the reduction in wounded area produced by NC was not statistically significant with respect to controls, the histological analysis of threated samples allowed an early re-epithelialization process (albeit limited to the lesion borders) and an advanced degree of hemostasis (with platelet plug) and angiogenesis (with reconstructed vasculature) to be demonstrated. Moreover the presence of granulation tissue was observed. After 18 days of treatments the overall skin structure was recovered showing even the regeneration of hair follicles.

#### References

- [1] S. Das, A. B. Baker, Biomaterials and Nanotherapeutics for Enhancing Skin Wound Healing, Front. Bioeng. Biotechnol. 4 (2016) 1-20
- [2] T.Velnar, T. Bailey, V. Smrkolj, The wound healing process: an overview of the cellular and molecular mechanisms, J. Int. Med. Res. 37 (2009) 1528-1542
- [3] A. J. Singer, R.A.F. Clark, Cutaneous wound healing, New Eng. J. Med. 341 (1999) 738-746
- [4] L.E. Smith, Modelling of cell-tissue interactions in skin, in : M.S. Agren (Ed.), Wound healing biomaterials Volume 2, Woodhead Publishing Duxford, 2016, pp. 39-54

- [5] P. Aramwit, Introduction to biomaterials for wound healing, in: M.S. Agren (Ed.), Wound healing biomaterials Volume 2, Woodhead Publishing Duxford, 2016, pp. 3-38
- [6] J. I. Dawson, R. O. C. Oreffo, Clay: new opportunities for tissue regeneration and biomaterial design, *Adv. Mat.* 25 (2013) 4069-4086.
- [7] G. Sandri, M. C. Bonferoni, S. Rossi, F. Ferrari, C. Aguzzi, C. Viseras, C. Caramella, Clay minerals for tissue regeneration, repair and engineering, in : M.S. Agren (Ed.), Wound healing biomaterials Volume 2, Woodhead Publishing Duxford, 2016, pp. 385-402
- [8] M. Kryuchkova, A. Danilushkina, Y. Lvov, R. Fakhrullin, Evaluation of toxicity of nanoclays and graphene oxide in vivo: a *Paramecium caudatum* study. *Environ. Sci.: Nano* 3 (2016) 442-452.
- [9] F. Cravero, G. J. Churchman, The origin of spheroidal halloysites: a review of the literature, *Clay Minerals* 51 (2016) 417-427
- [10] E. A. Naumenko, I. D. Guryanov, R. Yendluri, Y. M. Lvov, R. F. Fakhrullin, Clay nanotube-biopolymer composite scaffolds for tissue engineering, *Nanoscale* 8 (2016) 7257-7271
- [11] R. F. Fakhrullin, Y. M. Lvov, Halloysite clay nanotubes for tissue engineering, *Nanomedicine* 11 (2016) 2243-2246
- [12] E. Abdullayev, Y. Lvov, Halloysite clay nanotubes as a ceramic “skeleton” for functional biopolymer composites with sustained drug release. *J. Mater Chem. B*, 1 (2013) 2894-2903
- [13] Y. Lvov, E. Abdullayev, Functional polymer-clay nanotube composites with sustained release of chemical agent, *Prog. Polym. Sci.* 38 (2013) 1690-1719
- [14] Y. Lvov, W. Wang, L. Zhang, R. Fakhrullin, Halloysite clay nanotubes for loading and sustained release of functional compounds, *Adv. Mater.*, 28 (2016) 1227-1250
- [15] M. R. Dзамukova, E. A. Naumenko, Y. M. Lvov, R. F. Fakhrullin, Enzyme-activated intracellular drug delivery with tubule clay nanoformulation, *Sci Rep.* 5 (2015) 10560
- [16] R. Yendluri, D. O. Otto, M. M. De Villiers, V. Vinokurov, Y. M. Lvov, Application of halloysite clay nanotubes as a pharmaceutical excipient, *Int J. Pharm.* 521 (2017) 267-273
- [17] A. Fillipov, D. Afonin, N. Kononenko, Y. Lvov, V. Vinokurov, New approach to characterization of hybrid nanocomposites, *Col. Surf. A* 521 (2017) 251-259
- [18] Y. Lvov, M. M. De Villiers, R. F. Fakhrullin, The application of halloysite tubule nanoclay in drug delivery, *Exp Opin Drug Deliv.* 13 (2016) 977-986
- [19] C. Muanprasat, V. Chatsudthipong, Chitosan oligosaccharide: Biological activities and potential therapeutic applications, *Pharmacol. Ther.* 170 (2017) 80-97.

- [20] G. Lodhi, Y.-S. Kim, J.-W. Hwang, S.-K. Kim, Y.-J. Jeon, J.-Y. Je, C.-B. Ahn, S.-H. Moon, B.-T. Jeon, P.-J. Park, Chitooligosaccharide and Its Derivatives: Preparation and Biological Applications, *BioMed Research International*, 2014 (2014), Article ID 654913
- [21] C. Aguzzi, C. Viseras, P. Cerezo, I. Salcedo, R. Sánchez-Espejo, C. Valenzuela, Release kinetics of 5-aminosalicylic acid from halloysite, *Colloid Surface B*, 105 (2013) 75-80
- [22] C. Aguzzi, G. Sandri, C. Viseras, M. C. Bonferoni, P. Cerezo, S. Rossi, F. Ferrari, C. Caramella, Solid state characterisation of silver sulfadiazine loaded on montmorillonite/chitosan nanocomposite for wound healing, *Colloid Surface B*, 113 (2014) 152– 157
- [23] G. Sandri, M. C. Bonferoni, F. Ferrari, S. Rossi, C. Aguzzi, M. Mori, P. Grisoli, P. Cerezo, M. Tenci, C. Viseras, C. Caramella, Montmorillonite-chitosan-silver sulfadiazine nanocomposites for topical treatment of chronic skin lesions: in vitro biocompatibility, antibacterial efficacy and gap closure cell motility properties, *Carbohydr. Polym.* 102 (2014) 970–977
- [24] M.M. Leane, R. Nankervis, A. Smith, L. Illum, Use of the ninhydrin assay to measure the release of chitosan from oral solid dosage forms, *Int. J. Pharm.* 271 (2004), 241–249
- [25] S.R. Levis, P.B. Deasy, Characterisation of halloysite for use as a microtubular drug delivery system, *Int. J. Pharm.*. 243 (2002) 125–134
- [26] L. Liu, Y. Zhang, C. Wu, S. Xiong, C. Zhou, Chitosan/halloysite nanotubes bionanocomposites: structure, mechanical properties and biocompatibility, *Int. J. Biol. Macromol.* 51 (2012) 566-575

## Tables

Table 1

chitosan oligosaccharide/HNTs	R	chitosan oligosaccharide th (g)	HNTs th (g)	chitosan oligosaccharide tr %	HNTs tr %
R=0.5	0.5	0.1	0.2	0.277±0.097	99.723
R=0.4	0.4	0.1	0.25	0.001±0.021	99.999
R=0.2	0.2	0.1	0.5	0.336±0.067	99.664
R=0.1	0.1	0.1	1	1.025±0.059	98.975
R=0.075	0.075	0.1	1.33	1.339±0.015	98.661
R=0.05	0.05	0.1	2	1.365±0.045	98.635
R=0.025	0.025	0.1	4	0.932±0.021	99.068
R=0.0125	0.0125	0.1	8	0.780±0.047	99.220

## Figures

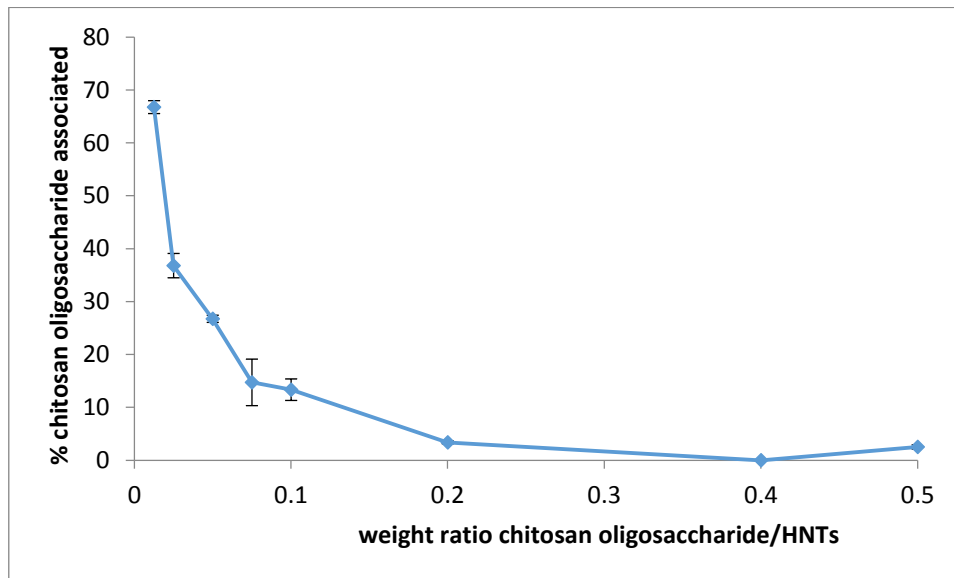


Figure 1

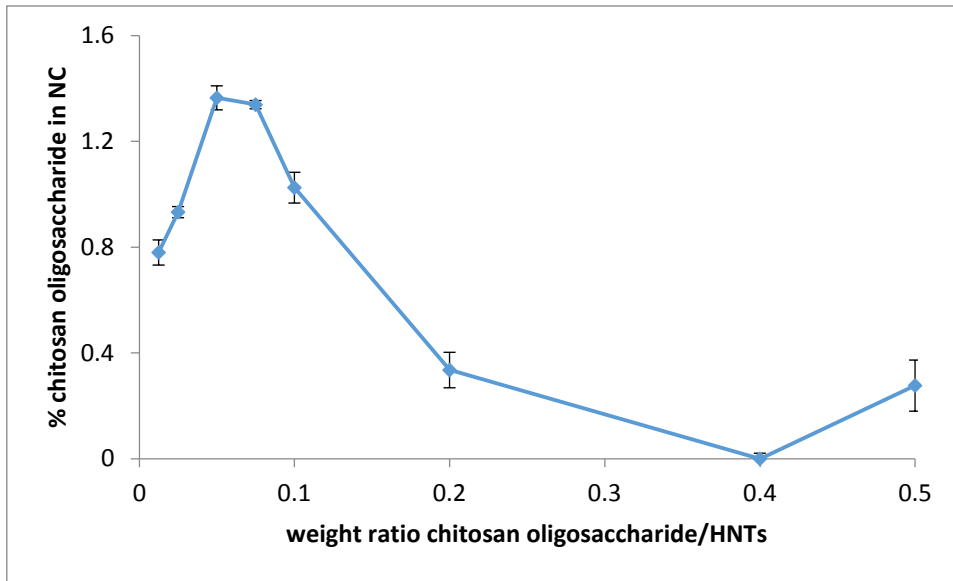


Figure 2

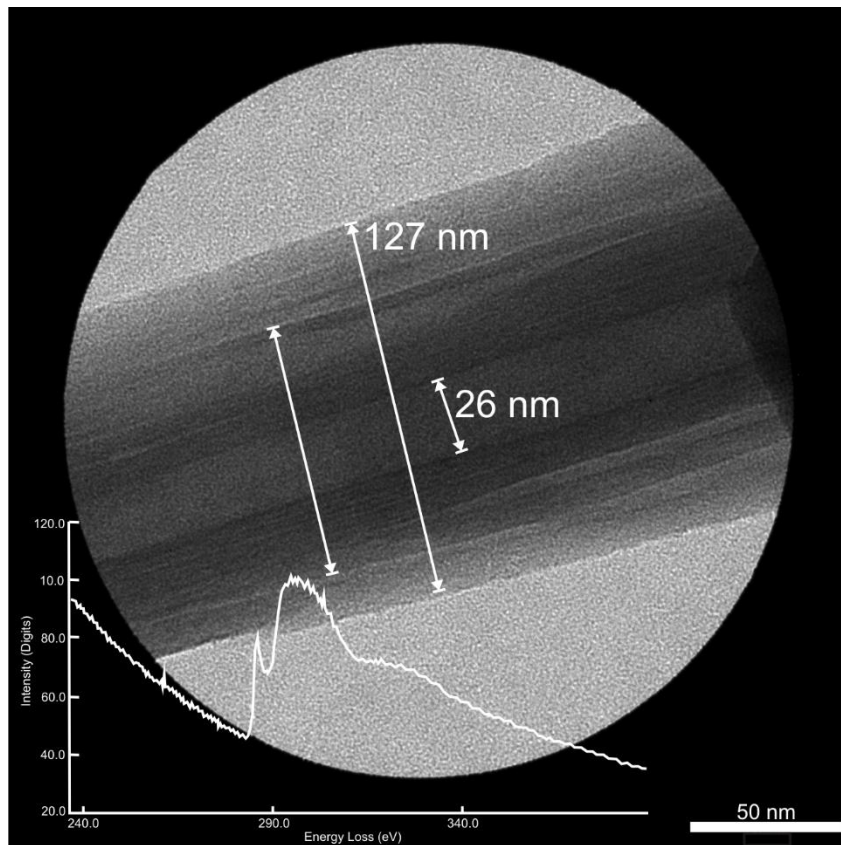


Figure 3

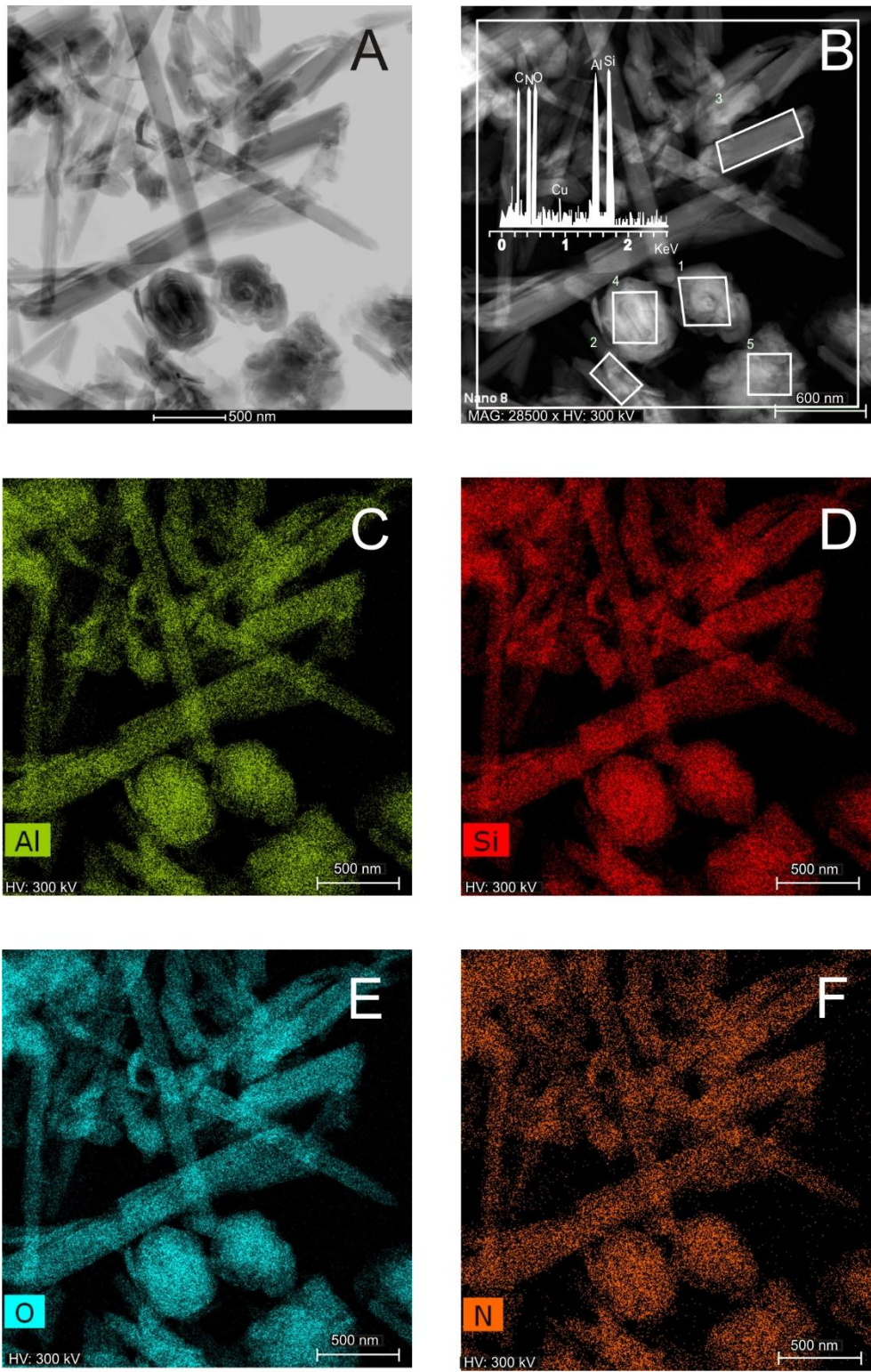


Figure 4

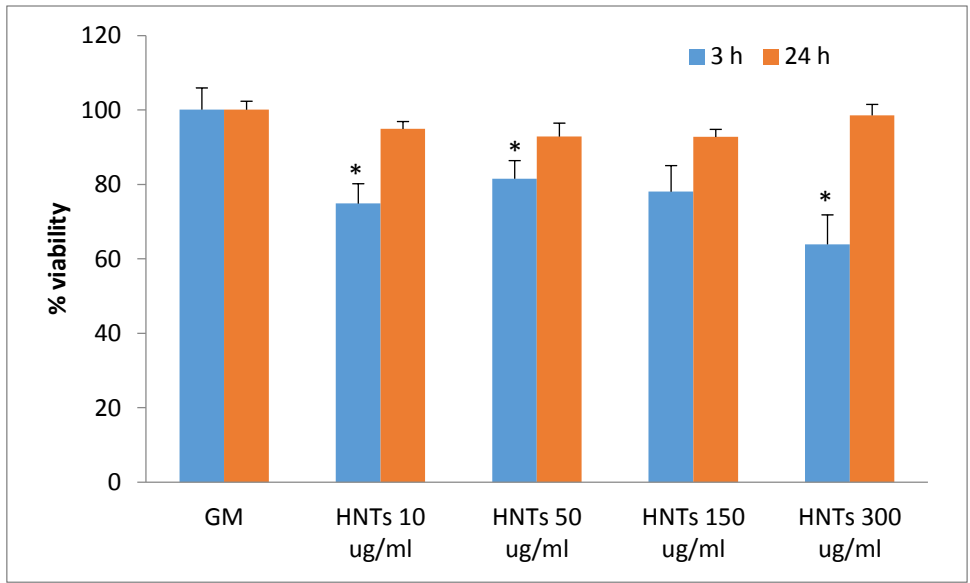


Figure 5

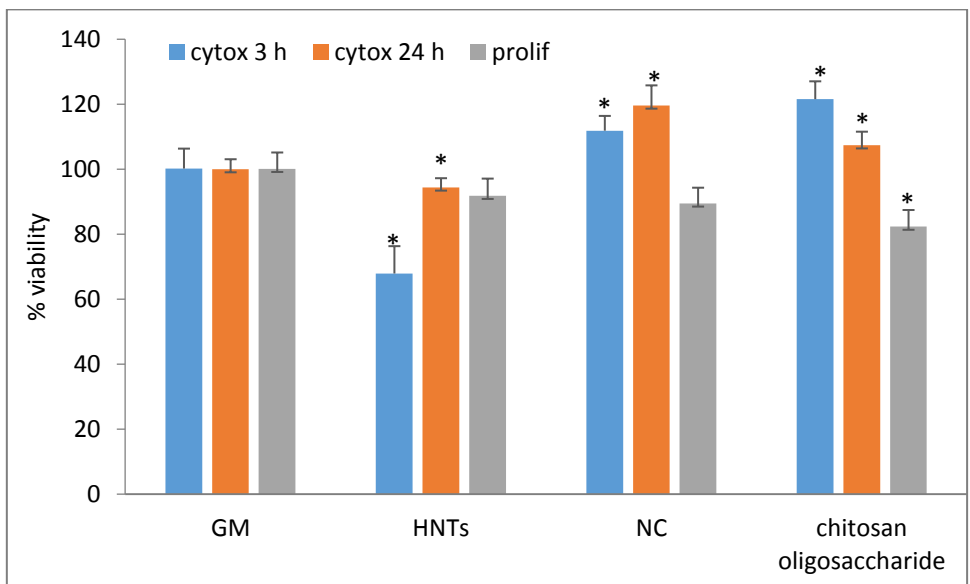


Figure 6

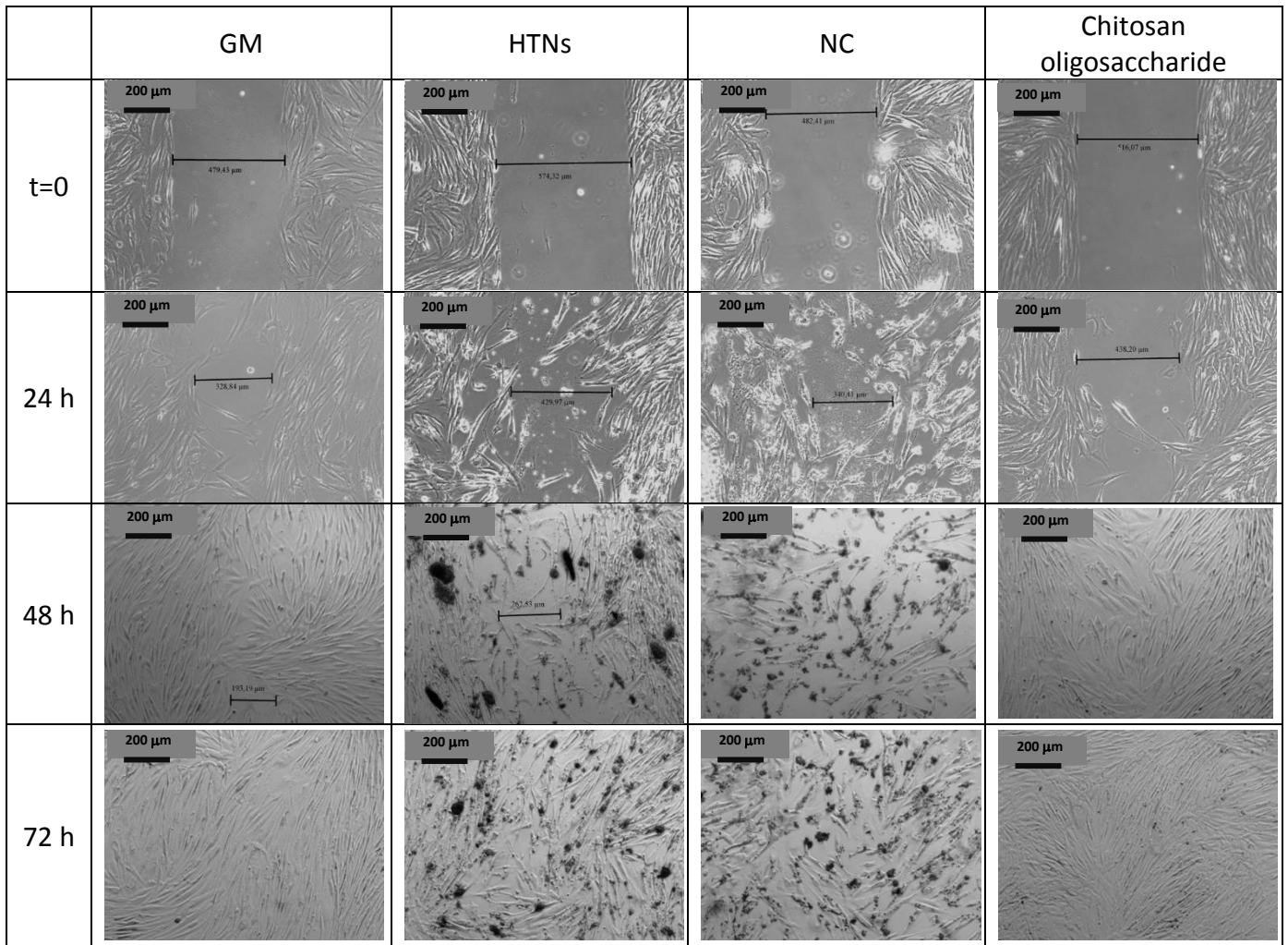


Figure 7

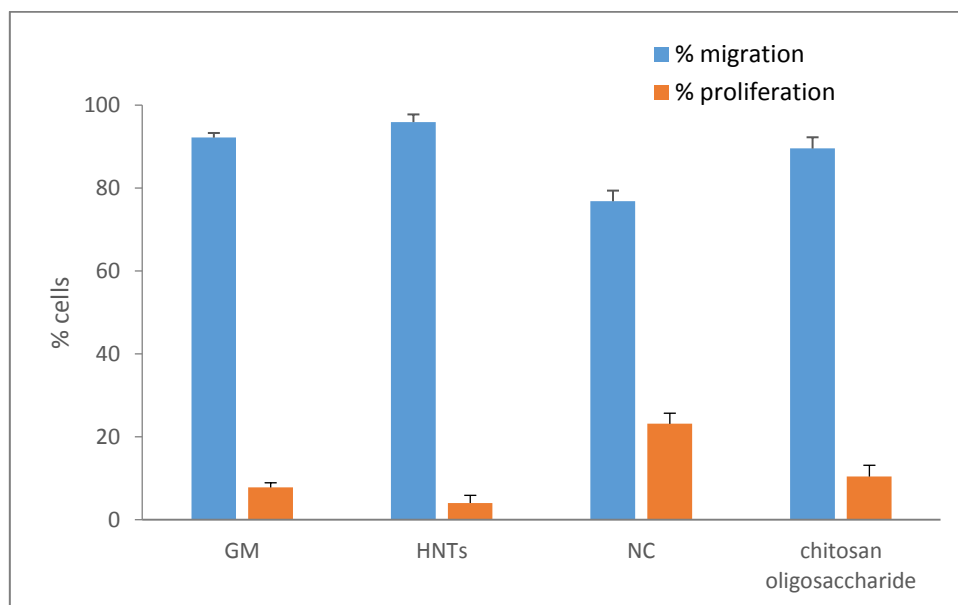


Figure 8



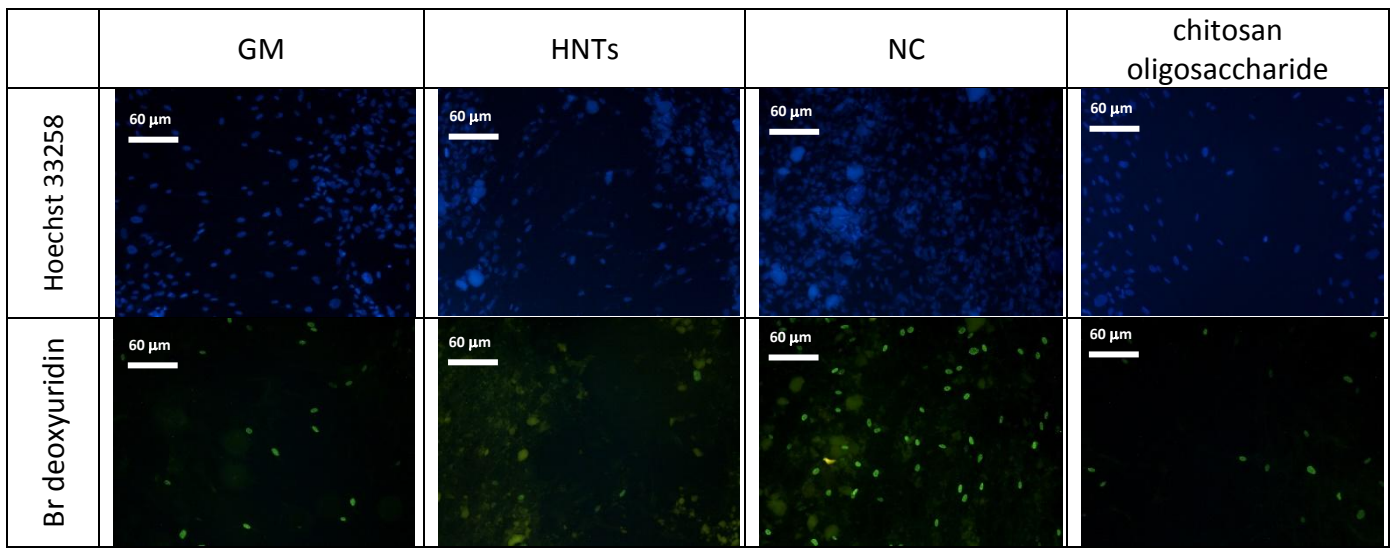


Figure 9

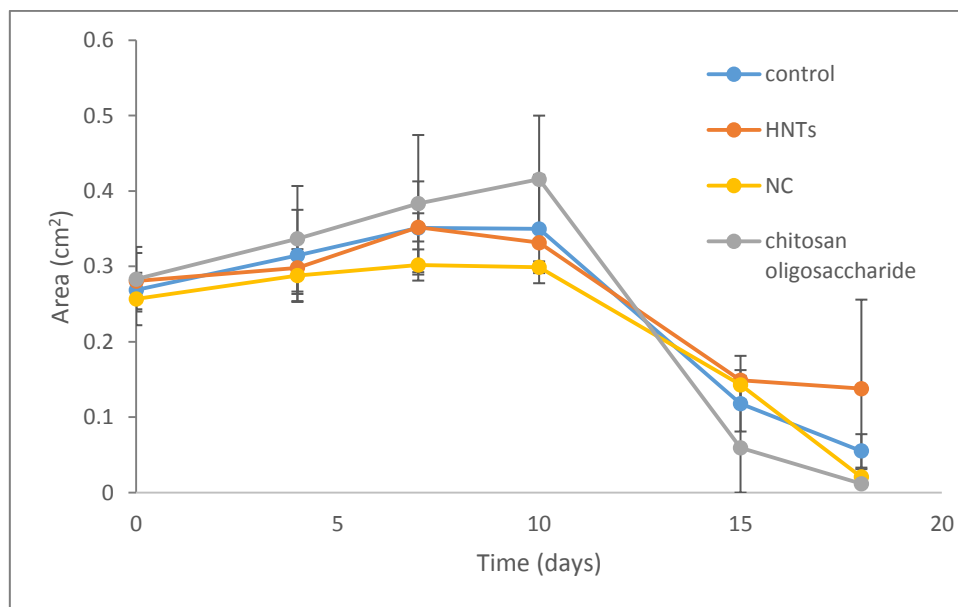


Figure 10

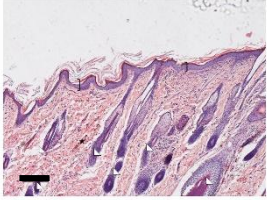
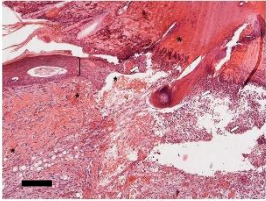
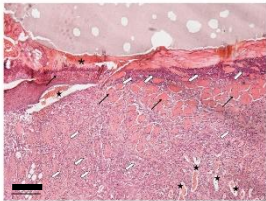
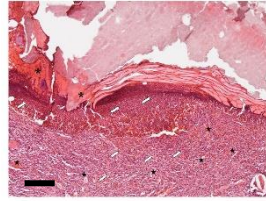
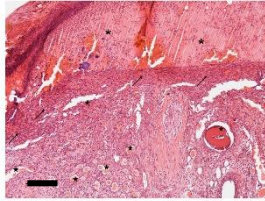
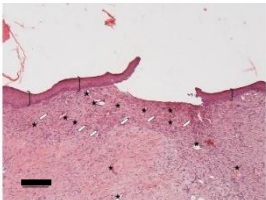
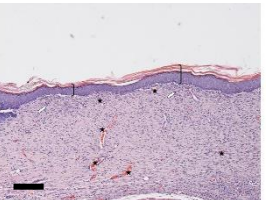
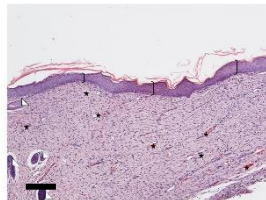
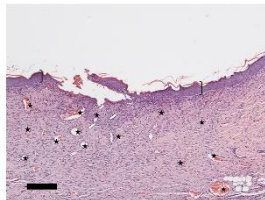
Intact skin				
	saline solution	HL	NC	COS
t=7				
t=14				

Figure 11

## Legends

Table 1: Quali quantitative composition of nanocomposites (th=theoric; tr=true) (mean values $\pm$ sd; n=6)

Figure 1: % of COS associated to HL nanocomposite vs COS/HL weight ratio (mean values $\pm$ sd; n=6)

Figure 2: % of COS contained in COS/HL nanocomposites vs COS/HL weight ratio(mean values $\pm$ sd; n=6)

Figure 3: Figure 3. TEM image (ESI mode) of a COS/HL nanotube and corresponding EELS spectrum.

Figure 4. TEM Microphotographs and chemical maps of COS/HL nanotubes. A) UHRTEM image; B) STEM image (type HAADF) detailing the areas analyzed by AEM and including one representative EDX spectrum; C-F) Al, Si, O and N X-Ray maps.

Figure 5: Cytotoxicity (% viability) of HL (concentrations ranging from 10 to 300  $\mu$ g/ml) after 3 or 24 h of contact times with normal human dermal fibroblasts (mean values $\pm$ sd; n=8) (\*  $p < 0.05$ )

Figure 6: Cytotoxicity after 3 or 24 h of contact times and in vitro proliferation (% viability) of 0.05 COS/HL nanocomposite NC (HL concentration 300  $\mu$ g/ml and COS concentration 4  $\mu$ g/ml), HL (concentration 300  $\mu$ g/ml) and COS (concentration 4  $\mu$ g/ml), towards normal human dermal fibroblasts (mean values $\pm$ sd; n=8) (\*  $p < 0.05$ )

Figure 7: Microphotographs of cell substrates subjected to in vitro wound healing test (samples: NC - 0.05 COS/HL nanocomposite (HL concentration 300  $\mu$ g/ml and COS concentration 4  $\mu$ g/ml); HL (concentration 300  $\mu$ g/ml); COS (concentration 4  $\mu$ g/ml); GM growth medium – standard growth conditions)

Figure 8: percentages of migrated (blue stained cells) and proliferating cells (blue and green stained cells) counted in the gaps of in vitro wound healing test (72 h of growth) associated with Br-deoxyuridine test (samples: NC - 0.05 COS/HL nanocomposite (HL concentration 300  $\mu$ g/ml and COS concentration 4  $\mu$ g/ml); HL (concentration 300  $\mu$ g/ml); COS (concentration 4  $\mu$ g/ml); GM growth medium – standard growth conditions) (mean values $\pm$ sd; n=8)

Figure 9: Microphotographs of cell substrates subjected to in vitro wound healing test associated with Br-deoxyuridine test (blue stained cells – migrated cells; blue and green stained cells - proliferating cells in S-phase) localized in the gaps (72 h of growth) (samples: NC - 0.05 COS/HL nanocomposite (HL concentration 300  $\mu$ g/ml and COS concentration 4  $\mu$ g/ml); HL (concentration 300  $\mu$ g/ml); COS (concentration 4  $\mu$ g/ml); GM growth medium – standard growth conditions)

Figure 10: in vivo lesion reduction vs time profile evaluated for the following samples NC - 0.05 COS/HL nanocomposite (HL concentration 300  $\mu$ g/ml and COS concentration 4  $\mu$ g/ml); HL (concentration 300  $\mu$ g/ml); COS (concentration 4  $\mu$ g/ml); saline solution – negative control) (mean values $\pm$ sd; n=8)

Figure 11: Light microphotographs of haematoxylin and eosin stained skin sections after 7 and 18 days of treatment with saline solution (negative control), HL, NC and COS. Intact tissue section is also reported. Skin structures are labelled as follows: epidermis = bracket; vessel = star; granulation tissue = pentagons; hair follicle = triangle; platelets = white arrow; necrotic tissue = asterisk, muscular fibers = arrow. Scale bar = 200  $\mu$ m